Electronic Supporting Information

Phase Behavior and Substitution Limit of Mixed Cesium-Formamidinium Lead Tri-iodide Perovskites

Bethan Charles[1], Mark T. Weller*[2], Sebastian Rieger[3], Lauren E. Hatcher[1], Paul F. Henry[4,5], Jochen Feldmann[3], Daniel Wolverson[1] and Chick C. Wilson[1]

[1]Centre for Sustainable Chemical Technologies, Departments of Chemistry and Physics, University of Bath, Bath BA2 7AY United Kingdom
[2]School of Chemistry, Cardiff University, Cardiff CF10 3AT, United Kingdom
[3]Chair for Photonics and Optoelectronics, Nano-Institute Munich, Department of Physics, Ludwig-Maximilians-Universität (LMU), Königinstr. 10, 80539 Munich, Germany
[4]Nanosystems Initiative Munich (NIM) and Center for NanoScience (CeNS), Ludwig-Maximilians-Universität (LMU), Schellingstr. 4, 80799 Munich, Germany
[5]ISIS Neutron and Muon Source, Rutherford Appleton Laboratory, Didcot, Oxfordshire OX11 0QX, United Kingdom
[6]Department of Chemistry and Chemical Engineering, Chalmers University of Technology, SE-412 96 Göteborg, Sweden

S1 – Additional Synthesis Details

Method	*x*	CsI (g)	FAI (g)	PbI_2 (g)	HI (ml)	GBL (ml)
Precipitation[1]	0.15	0.0603	0.2262	0.7135	1.55	0
	0.2	0.0799	0.2115	0.7087	1.54	0
Inverse Solubility[2]	0.15	0.0603	0.2262	0.7135	0	1.72
	0.2	0.0799	0.2115	0.7087	0	1.71

Table S1 Reactant quantities used in the synthesis of $Cs_xFA_{1-x}PbI_3$ (x = 0.15, 0.2) via the precipitation and inverse solubility methods.

S2 – Sample Composition from EDX

The composition of single crystals of $Cs_{0.1}FA_{0.9}PbI_3$ grown via inverse solubility were analyzed using energy dispersive x-ray spectroscopy (EDX). Cs was distributed throughout the whole of the sample with the average weight % of Cs measured via EDX being 2.42% corresponding to a composition of $Cs_{0.12}FA_{0.88}PbI_3$.

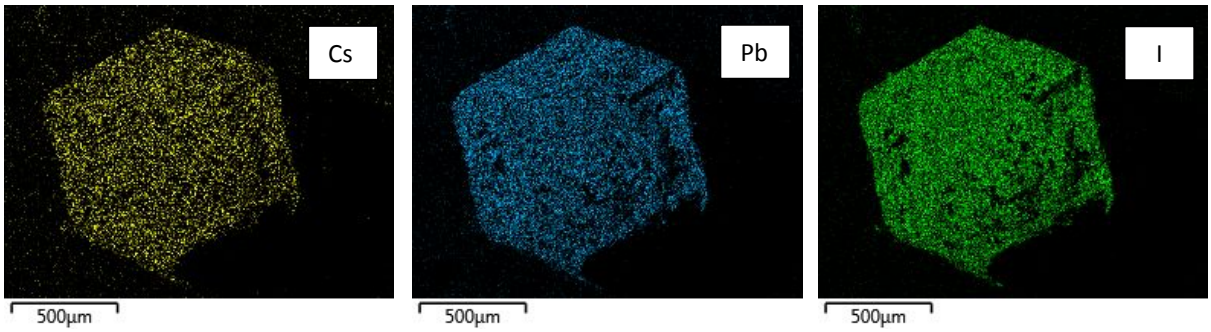

Figure S1 EDX maps of mixed Cs/FA lead iodide perovskite crystals grown via inverse solubility showing distribution of Cs (yellow), Pb (blue) and I (green).

S3 – Phase Separation Above Cs Substitution Limit

Crystals and powders $Cs_xFA_{1-x}PbI_3$ ($0 < x \leq 0.2$) were synthesized using the inverse solubility and precipitation techniques respectively, however, compositions of $x \geq 0.2$ showed significant phase separation into perovskite α and non-perovskite δ-phases.

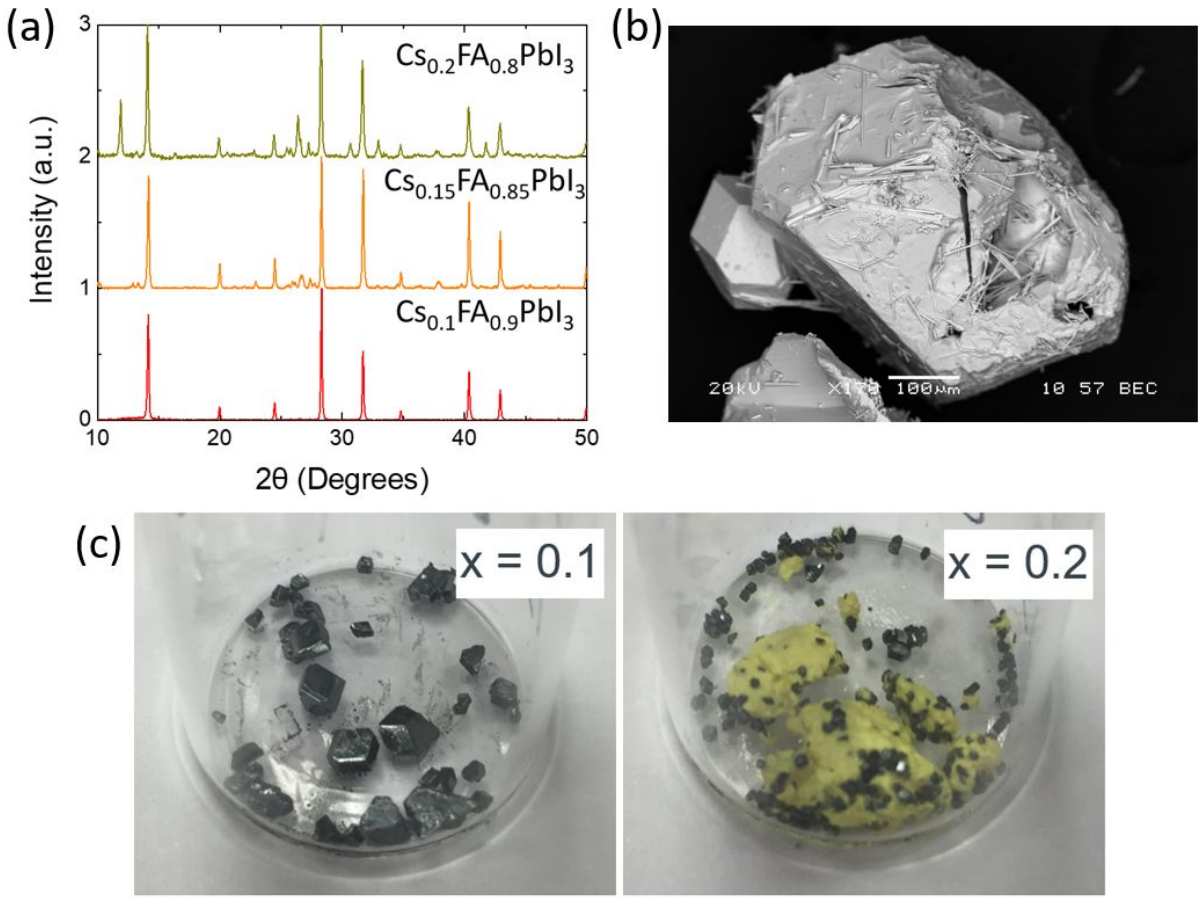

Figure S2 (a) Powder X-ray diffraction (PXRD) patters for samples of $Cs_xFA_{1-x}PbI_3$ (x = 0.1, 0.15, 0.2) grown via inverse solubility. Additional peaks in the $Cs_{0.15}FA_{0.85}PbI_3$ and $Cs_{0.2}FA_{0.8}PbI_3$ patterns could be assigned to the non-perovskite δ-phases of $FAPbI_3$ and $CsPbI_3$. (b) Backscattered scanning electron microscope (SEM) image of $Cs_{0.2}FA_{0.8}PbI_3$ crystal, needles of the δ-phases can be seen across the crystal surface. (c) Images of as-made $Cs_xFA_{1-x}PbI_3$ (x = 0.1, 0.2) synthesized via inverse solubility.

S4 – Sample Purity

$Cs_{0.1}FA_{0.9}PbI_3$ samples grown by inverse solubility were phase pure; however, powders synthesized by the precipitation methods has small amounts (< 2%) of δ-phase impurities.

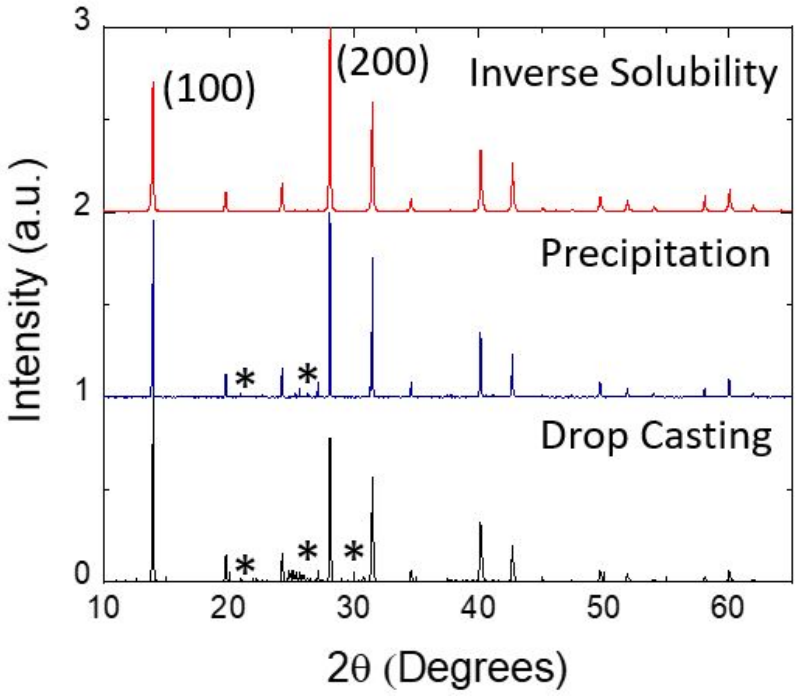

Figure S3 PXRD patterns of $Cs_{0.1}FA_{0.9}PbI_3$-H samples synthesized via inverse solubility (red), precipitation (blue) and $Cs_{0.1}FA_{0.9}PbI_3$-D synthesized by drop casting (black). The samples synthesized by the inverse solubility method were identified as phase pure, whereas small quantities of δ-$CsPbI_3$ and δ-$FAPbI_3$ impurities were identified in the other samples (identified by *).

S5 – Additional Crystallographic Information

Table S2 Refined positions and displacement parameters for partially deuterated α-$Cs_{0.1}FA_{0.9}PbI_3$-D from POLARIS data at 300 K, space group P$m\bar{3}m$, lattice parameter a = 6.34562(24) Å, wR = 1.68%. The central cation was modelled as a CH – NHD rigid molecule. Full CIF CsFA19_300_2h_4.cif

Atom	x	y	z	U_{iso} (Å^2)	Occupancy	Site Symmetry
Pb1	0	0	0	0.0255(13)	1.000	m3m
I1	0.5	0	0	0.0806(21)	1.000	4/mmm(x)
C1	0.5	0.50(12)	0.5	0.244(6)	0.167	4mm(y)
N1	0.70(11)	0.558(23)	0.5	= C1 U_{iso}	0.083	m(z)
H1	0.5	0.7(4)	0.5	= C1 U_{iso}	0.167	4mm(y)
H2	0.75(5)	0.65(7)	0.5	= C1 U_{iso}	0.083	m(z)
D1	0.7(4)	0.3(4)	0.5	= C1 U_{iso}	0.083	m(z)

Table S3 Refined positions and displacement parameters for partially deuterated β-$Cs_{0.1}FA_{0.9}PbI_3$-D from POLARIS data at 200 K, space group P4/*mbm*, lattice parameters *a* = 8.9084(8) Å *c* = 6.3224(8) Å, *w*R = 2.90%. The central cation was modelled as a CH – NHD rigid molecule. Full CIF CsFA19_200_2.cif

Atom	x	y	z	U_{iso} (Å^2)	Occupancy	Site Symmetry
Pb1	0	0	0	0.0057(22)	1	4/m(z)
I1	0	0	0.5	0.035(8)	1	4/m(z)
I2	0.7879(10)	0.28791	0	0.059(8)	1	mm2(xy)
C1	0.5	0	0.49(5)	0.190(9)	0.5	mm2(d001)
N1	0.57(17)	0.08(16)	0.42(3)	= C1 U_{iso}	0.25	1
H1	0.583(12)	0.91719	0.56(3)	= C1 U_{iso}	0.25	m(xy)
H2	0.54(7)	0.10(8)	0.45(13)	= C1 U_{iso}	0.25	1
D1	0.60(20)	0.11(19)	0.48(9)	= C1 U_{iso}	0.25	1

S6 – Differential Scanning Calorimetry

Differential scanning calorimetry (DSC) measurements for $Cs_{0.1}FA_{0.9}PbI_3$ samples synthesized via precipitation were cycled from 293 K – 225 K – 420 K four times at 2 K/min. A small transition of 0.01 W/g was observed centered at 290 K cycling down and 285 K cycling up in temperature corresponding to the phase transition from cubic to tetragonal. A 5 K difference in transition temperature between the down and up temperature cycles demonstrates he presence of a small amount of thermal hysteresis.

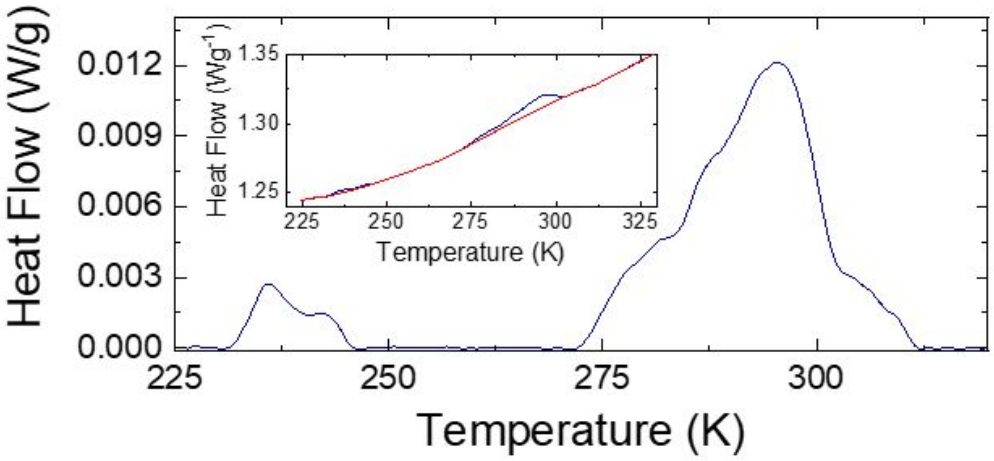

Figure S4 Baselined DSC measurement for $Cs_{0.1}FA_{0.9}PbI_3$ samples synthesized via inverse solubility cycled once between 293K – 225K – 420K at 2Kmin^{-1}. A very small change in heat flow is centered at 290K corresponding with the cubic to tetragonal phase transition, the same as that seen for samples synthesized via precipitation. (Inset) original data (blue) and baseline (red), the slope is an artifact of the instrument.

S7 – Photoluminescence Modelling

Steady state photoluminescence (PL) spectra were fitted with Gaussian functions, as shown in Figure S8a. Time-resolved PL were fitted according to the charge-carrier recombination rate equation:

$$-\frac{dn}{dt} = k_1 n + k_2 n^2 \quad \text{(S1)}$$

where n is charge carrier density, k_1 is the monomolecular rate constant and k_2 is the bimolecular rate constant. The analytical solution of this differential equation is given by:

$$n(t) = \frac{-k_1 \cdot exp\,(ck_1)}{k_2 \cdot exp\,(ck_1) - exp\,(k_1 t)} \quad (S2)$$

As we assume free carrier recombination and every recombination requires an electron and a hole, the measured signal $I(t)$ was taken to be proportional to $n(t)^2$:

$$n(t)^2 \propto I(t) \quad \text{(S2)}$$

Consequently, one must be aware of the fact that one can only extract a value called Bk_2 from the PL data where B is a proportionality constant as described by Milot *et al*.[4] As B is unknown, only the value of k_1 can be directly determined. Effective bimolecular rate constants are determined as Bk_2 with units of V ns^{-1}, where V is volume.

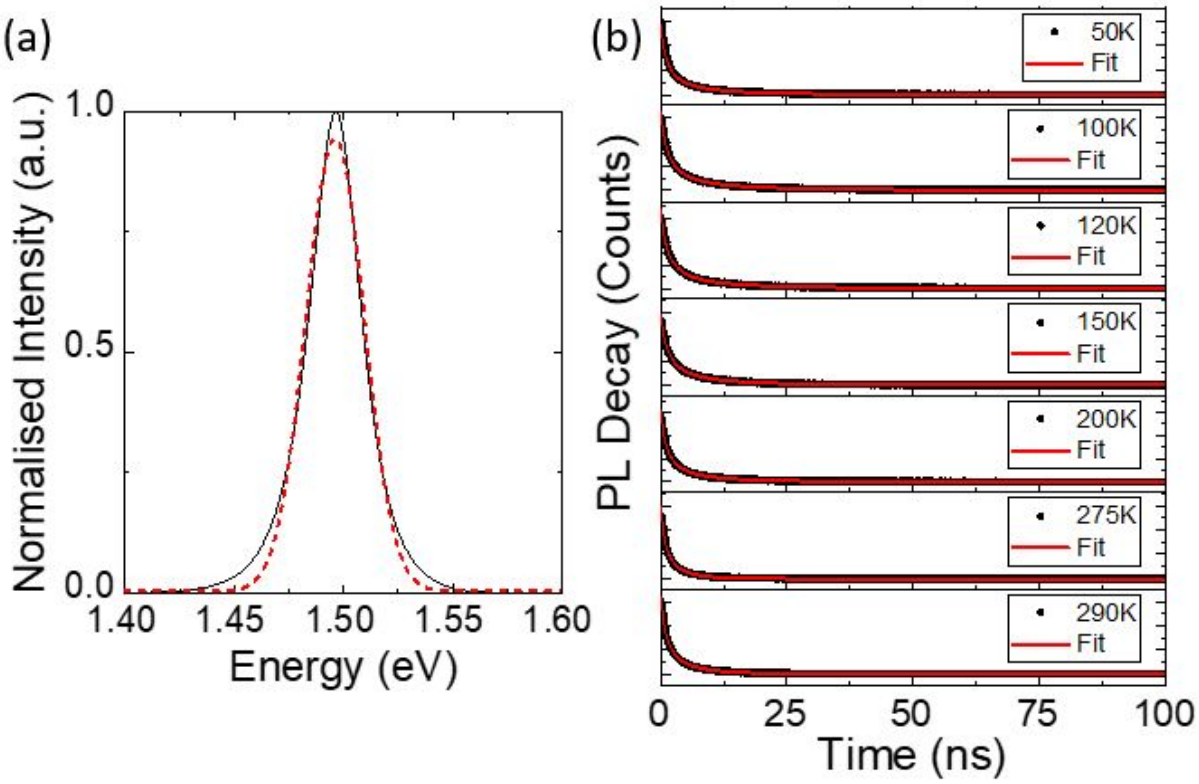

Figure S5 (a) Gaussian fit (red dashed line) of PL (black solid line) for a crystal of $Cs_{0.1}FA_{0.9}PbI_3$ taken at 50 K. (b) PL decay for $Cs_{0.1}FA_{0.9}PbI_3$ crystal (black) taken between 275 K and 50 K fitted according to equation S1.

S8 – Sample Stability

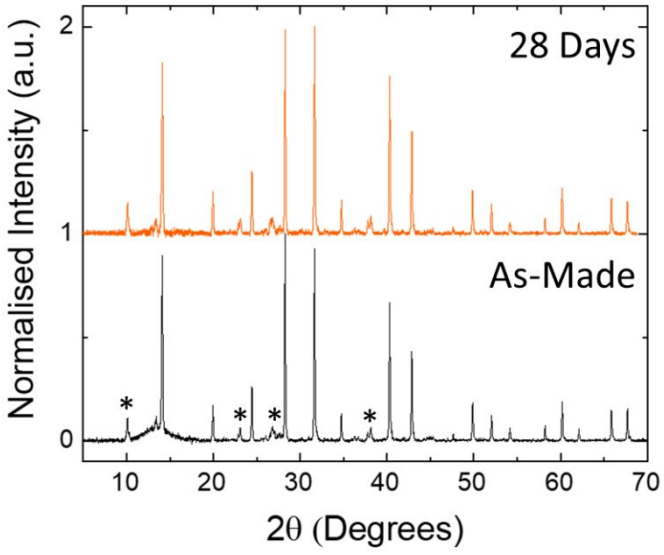

Figure S6 PXRD patterns of $Cs_{0.1}FA_{0.9}PbI_3$ samples synthesised by precipitation. Powder samples synthesised by precipitation would remain stable in air at 20% humidity over 28 days (* identifies δ-phase impurities in the as-made sample).

S9 – Sequential Refinement

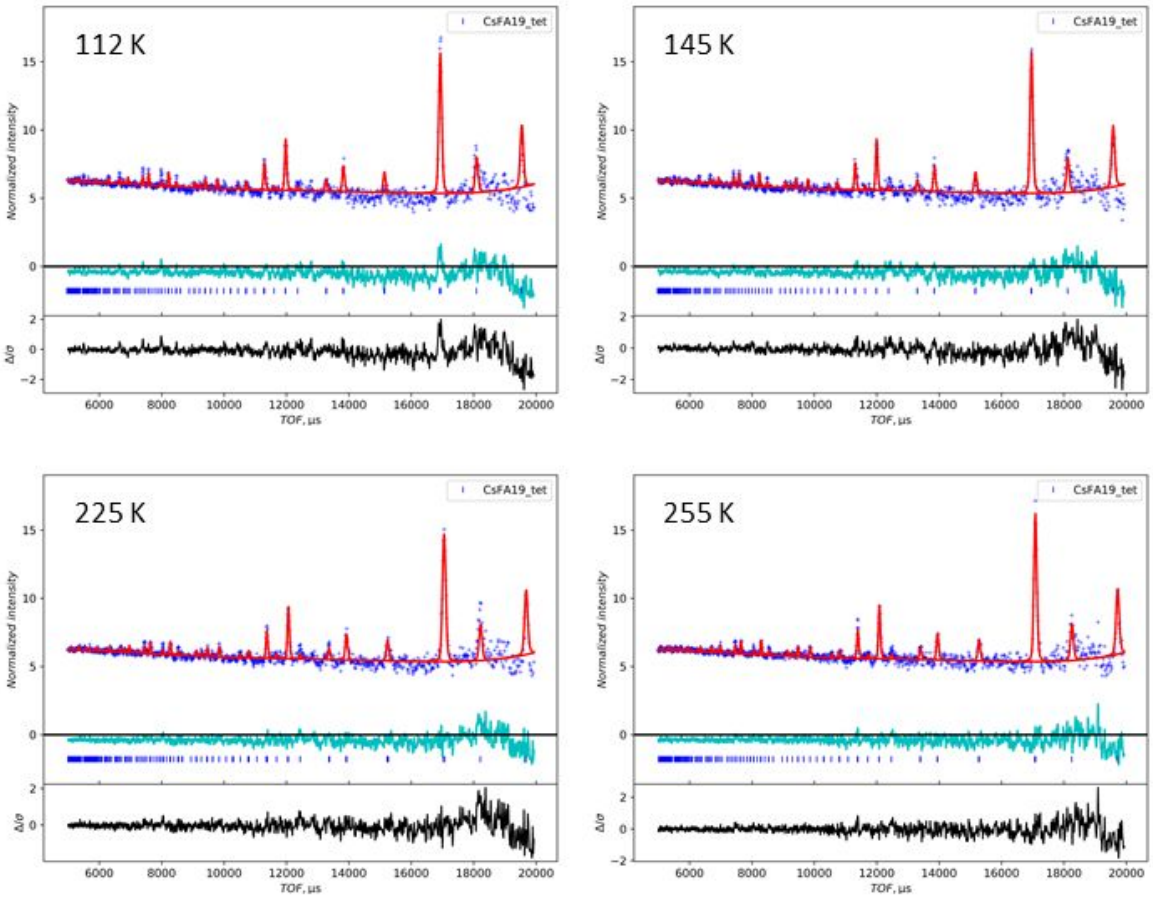

Figure S7 Example NPD patterns of $Cs_{0.1}FA_{0.9}PbI_3$ used in the sequential refinement producing the trend in pseudo-tetragonal lattice parameters shown in Figure 1b. Overall, 144 of these refinements were performed on NPD data between 280 K and 110 K.

S10 Generated (pseudo-) SXD precession figures for the 300 K cubic phase.

(a) hk0 layer

(b) h0l layer and

(c) (c) 0kl layer.

Figures are part labelled with (hkl) values.

(a)

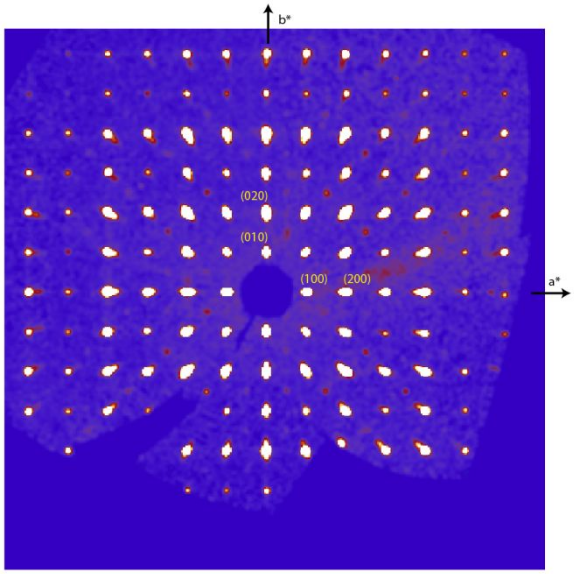

(b)

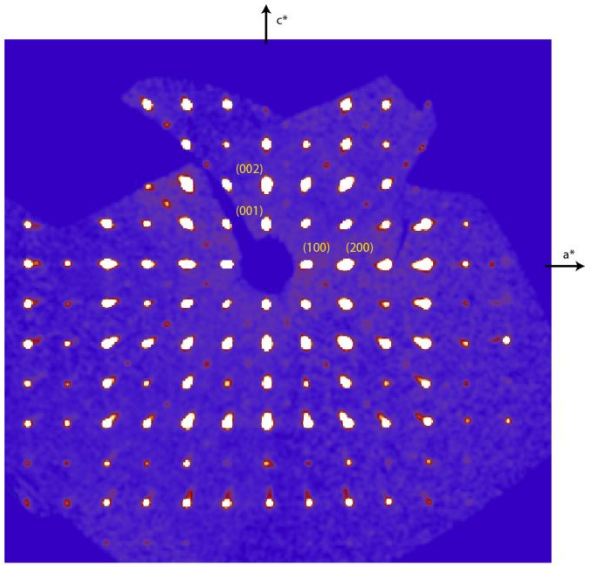

(c)

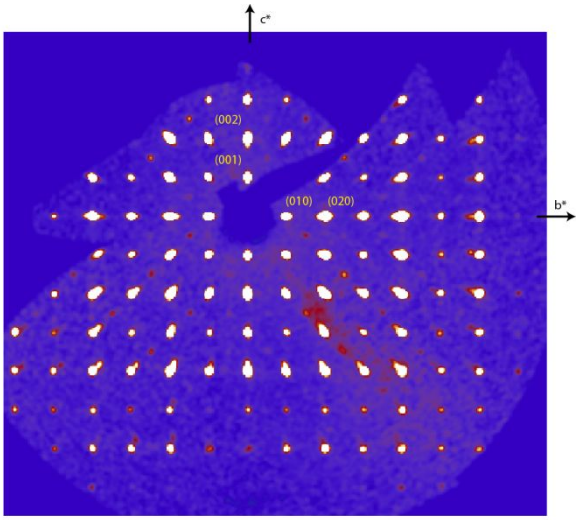

References

(1) Poglitsch, A.; Weber, D., Dynamic disorder in methylammoniumtrihalogenoplumbates (II) observed by millimetre-wave spectroscopy. *J. Chem. Phys*., **1987**, 87 (11), 6373

(2) Saidaminov, M. I.; Abdelhady, A. L.; Murali, B.; Alarousu, E.; Burlakov, V. M.; Peng, W.; Dursun, I.; Wang, L.; He, Y.; Maculan, G.; Goriely, A.; Wu, T.; Mohammed, O.F.; Bakr, O.M.; High-quality bulk hybrid perovskite single crystals within minutes by inverse temperature crystallization *Nat. Comm*., **2015**, 6, 7586

(3) Manser, J. S.; Kamat, P. V. Band filling with free charge carriers in organometal halide perovskites. *Nat. Photonics*, **2014**, 8 (9), 737-743

(4) Milot, R. L.; Sutton, R. J.; Eperon, G. E.; Haghighirad, A. A.; Martinez Hardigree, J.; Miranda, L.; Snaith, H. J.; Johnston, M. B.; Herz, L. M. Charge-Carrier Dynamics in 2D Hybrid Metal–Halide Perovskites. *Nano Lett*., **2016**, 16(11), 7001-7007